Geochemical Journal, Vol. 42, pp. 461 to 479, 2008

^{238}U–^{230}Th radioactive disequilibrium in the northern Izu arc: ($^{230}Th/^{232}Th$) in the sub-arc mantle

SATORU FUKUDA,[1] SHUN'ICHI NAKAI,[1]* KENJI NIIHORI,[1,2] MASASHI TSUKUI,[2] SETSUYA NAKADA,[1] TOSHITSUGU FUJII[1] and KENICHIRO TANI[3]

[1]Earthquake Research Institute, The University of Tokyo, Tokyo 113-0032, Japan
[2]Department of Earth Sciences, Faculty of Science, Chiba University, Inage-ku, Chiba 263-8522, Japan
[3]Institute for Frontier Research on Earth Evolution, Japan Agency for Marine-Earth Science and Technology, 2-15, Natsushima-cho, Yokosuka, Kanagawa 237-0061, Japan

(*Received September 12, 2007; Accepted May 30, 2008*)

Major and trace element abundances, Sr and Nd isotopic ratios, and ^{238}U–^{230}Th radioactive disequilibria have been analyzed for samples from five volcanoes, Oshima, Miyakejima, Niijima, Teishi Knoll and Fuji, located in the northern Izu arc to investigate across-arc and regional variations of chemical compositions of mantle and fluids expelled from a subducting slab. The abundances and abundance ratios of both fluid mobile and immobile trace elements show across-arc variations.

All samples but one have radioactive disequilibria, with ($^{238}U/^{230}Th$) greater than unity (herein, a ratio in parentheses denotes the activity ratio). The observed disequilibrium is similar to those reported for other arc systems, such as Mariana, Tonga, Kermadec, Chile. It originates from higher mobility of uranium relative to thorium during dewatering of the subducting slab. The degree of radioactive disequilibrium of ($^{238}U/^{230}Th$) decreases with depth to the Wadati-Benioff zone at each volcano. The radioactivity ratios of ($^{230}Th/^{232}Th$) of the samples from Miyakejima, however, deviate from an across-arc trend formed by Oshima, Niijima, Teishi Knoll and Fuji.

The combined data of ($^{230}Th/^{232}Th$)–($^{238}U/^{232}Th$) of the samples from the Izu and the Mariana arc revealed a well defined array in an isochron diagram with the exceptions of the samples from Miyakejima and Alamagan. This finding requires ($^{230}Th/^{232}Th$) of the sub-arc mantle beneath the arcs of Izu and Mariana except the magma sources of the two islands of Miyakejima and Alamagan was around 1.1 and relatively homogeneous before the final addition of fluid from slab. The homogeneous ($^{230}Th/^{232}Th$) necessitates input of Th with homogeneous ($^{230}Th/^{232}Th$) contributed from sediment melt, which dominates the budget of Th in the sub-arc mantle. It also suggests that influence of fluid addition before the final one had not caused a variation in Th isotopic compositions of the sub-arc mantle.

Keywords: U-series disequilibria, Izu arc, subduction, isotope geochemistry, trace element geochemistry, sediment

INTRODUCTION

To date, ^{238}U–^{230}Th radioactive disequilibrium has been used to infer time constraints on arc volcanisms (Hawkesworth *et al*., 2004; Turner *et al*., 2003). Such studies describe a radioactive disequilibrium observed in arc-derived volcanic rocks—e.g., ($^{238}U/^{230}Th$) greater than unity—and ascribe the disequilibrium to the chemical fractionation of fluid mobile uranium from immobile thorium during dehydration. The U addition time scales have been estimated from sets of along-arc samples, which form an inclined array in the ($^{230}Th/^{232}Th$)–($^{238}U/^{232}Th$) isochron diagram. Elliot *et al*. (1997), for example, described a clear array formed by volcanic rocks from the Mariana arc, which can be interpreted to record a uranium addition event at 30 ka prior to eruption if mantle homogeneity regarding ($^{230}Th/^{232}Th$) and negligible thorium addition by fluid can be assumed. This approach reveals that samples from about 15 arcs record fluid addition events that occurred 10–200 kyr prior to eruption (Turner *et al*., 2003). Most prior studies of the radioactive disequilibria on island-arc derived volcanic rocks have mostly investigated samples from different volcanoes from an arc as the dataset of the arc, although several volcanoes have been intensively investigated (Yokoyama *et al*., 2003, 2006; George *et al*., 2004; Jicha *et al*., 2005; Tepley *et al*., 2006). For this approach to be possible to give accurate time scale of magma ascent, the mantle wedge should have had a homogeneous Th radioactivity ratio before the final fluid addition.

For the present study, we analyzed major and trace element abundances and U–Th radioactive disequilibria with Sr and Nd isotopes of volcanic rocks from the Izu

*Corresponding author (e-mail: snakai@eri.u-tokyo.ac.jp)

arc. This arc has been investigated using various chemical and isotopic tracers. Across-arc variations of fluid-derived components have been reported by many authors (Tatsumi *et al*., 1992; Ishikawa and Nakamura, 1994; Moriguti and Nakamura, 1998; Taylor and Nesbitt, 1998; Straub and Layne, 2002; Ishizuka *et al*., 2003, 2006).

Taylor and Nesbit (1998) reported considerable along-arc variation in Sr, Nd and Pb isotopes in the Izu arc. They attributed variations of Sr and Pb isotopes to fluid addition processes. In addition, they concluded that variations in Nd isotopes indicate that heterogeneity existed within the sub-arc mantle prior to enrichment by the subduction fluids. Hochstaedter *et al*. (2000, 2001) and Machida and Ishii (2003), using trace element abundance data for the southern Izu arc, have suggested mantle heterogeneity. Ishizuka *et al*. (2003) identified a systematic along-arc isotopic variation of lavas in back-arc region of the Izu arc as well as in the volcanic front of the arc. Ishizuka *et al*. (2006), furthermore, presented isotopic variation with time in the Izu arc. These findings clearly demand a study on U–Th radioactive disequilibria in the Izu arc.

Yokoyama *et al*. (2003) analyzed the ^{238}U–^{230}Th–^{226}Ra disequilibria of the samples from Miyakejima in the northern Izu arc. Yokoyama *et al*. (2003) estimated ($^{230}Th/^{232}Th$) of the mantle beneath Miyakejima at 1.30. This work will report radioactive disequilibrium data on the volcanoes from the northern Izu arc, including Miyakejima, and will present discussion of the variation of Th isotopic ratio within the arc system with comparison to data of Yokoyama *et al*. (2003). We will further compare our data with those from the Mariana arc (Elliott *et al*., 1997).

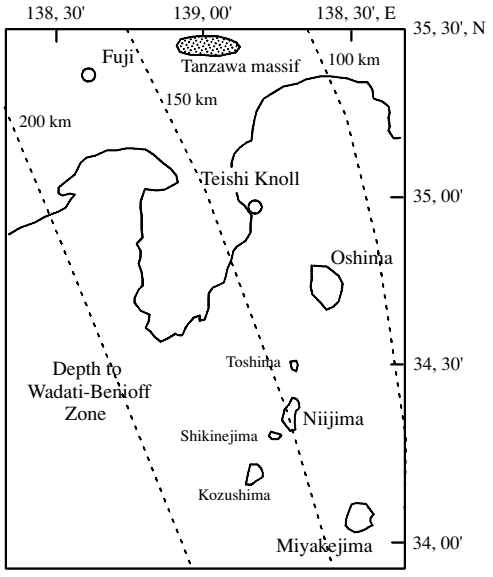

Fig. 1. Map of northern part of the Izu arc. The dashed lines indicate the depth contours of the upper surface of the Pacific Plate, as described in Nakajima and Hasegawa (2006). The locations of the five volcanoes and the Tanzawa massif are shown as the hatched area.

Samples and Analytical Methods

Samples

We analyzed volcanic rock samples from Oshima, Miyakejima, Niijima, and Teishi Knoll off the coast of Izu peninsula, and Fuji (Fig. 1). We selected these volcanoes because they are distributed in the northern Izu island arc with various depths to the subducting slab. Nakajima and Hasegawa (2006) presented the iso-depth contours of the subducted Pacific plate based on the precisely determined hypocenter distribution obtained in Kanto-Tokai district. Using their iso-depth contours, we estimated the depth to Wadati-Benioff Zone as 120 km at Oshima, 130 km at Miyakejima, 140 km at Teishi Knoll, 150 km at Niijima, and 160 km at Fuji (Fig. 1). Most samples are basalt or basaltic andesite. The eruption ages of the samples from Fuji, Miyakejima and Oshima were estimated by historic records, tephrochronological methods and the ^{14}C method as younger than 3000 years (Miyaji, 1988; Yoshimoto *et al*., 2004; Tsukui *et al*., 2001; Niihori *et al*., 2003; Nakamura, 1964). Descriptions of the samples of 2000 eruption of Miyakejima are in Amma-Miyasaka *et al*. (2005) and Kaneko *et al*. (2005). The age of Nij from Niijima was estimated from archaeological objects and a ^{14}C age (Isshiki, 1987). We analyzed only one sample for Niijima because only one sequence of lava with basaltic composition is present on the island. Monogenic volcanoes are distributed around the eastern part of the Izu peninsula (Hamuro, 1985). The sample of volcanic ejecta from the Teishi Knoll was recovered when a submarine eruption occurred off the coast of the Izu Peninsula in 1989 (Yamamoto *et al*., 1991).

The gabbro and tonalite samples were collected from the Tanzawa plutonic complex, located north of the studied area. They were analyzed to evaluate the influence of crustal contamination.

Analytical techniques

All samples were crushed with an agate mortal to powder. Wakagou basalt in Niijima contained rhyolite inclusions (<1 mm). These inclusions were removed under a microscope before crushing. For this study, we did not leach sample powders using an acid solution, thereby avoiding selective leaching, which causes U/Th fractionation of a sample. Instead, in order to remove surface contamination and possible seawater contamination, sample tips were washed in a Milli-Q water ultrasonic bath.

Table 1. Chemical and isotopic compositions of Izu arc samples

	Fuji				Miyakejima					
	JB3	SJ77	SJ70	Ho-IV	KSL	TYL	1469	1643	1763	1874
Eruption age	864	937	1033	1707	2200–3000	2050	1469	1643	1763	1874
SiO_2(%)	51.03	51.61	51.49	51.49	58.16	52.11	53.55	52.84	54.45	54.03
TiO_2	1.43	1.34	1.29	1.35	1.16	1.28	1.29	1.39	1.38	1.28
Al_2O_3	17.08	18.43	17.75	17.13	14.99	15.16	15.01	14.63	14.60	15.72
FeO	11.84	10.16	10.32	10.85	10.94	13.26	12.86	13.76	13.15	12.07
MnO	0.18	0.17	0.17	0.19	0.23	0.24	0.24	0.25	0.24	0.23
MgO	5.18	4.61	5.57	5.29	3.02	4.98	4.55	4.54	3.99	4.09
CaO	9.79	9.99	9.76	9.71	7.32	9.97	9.24	9.35	8.59	9.15
Na_2O	2.68	2.84	2.78	2.68	3.36	2.46	2.55	2.59	2.83	2.72
K_2O	0.77	0.71	0.69	0.73	0.65	0.41	0.56	0.50	0.59	0.56
P_2O_5	0.29	0.26	0.26	0.26	0.15	0.12	0.15	0.15	0.16	0.15
Rb (ppm)	12.8	14.59	12.8	13.3	8.48	5.07	7.90	7.49	8.86	7.72
Sr	377	395.24	405	404	248	231	239	247	256	244
Zr	100	83.8	80.6	73.6	71.1	45.2	66.4	63.0	72.2	66.3
Nb	2.12	1.91	1.71	1.66	0.66	0.41	0.60	0.60	0.68	0.64
Cs	0.83	0.99		0.91	0.66	0.38	0.60		0.68	0.58
Ba	216	226	216	230	238	148	207	200	237	206
La	7.52	7.96	7.45	7.51	4.12	2.53	3.71	3.45	4.08	3.66
Ce	19.5	20.2	19.8	20.1	12.0	7.7	10.8	10.04	12.2	10.9
Pr	2.89	3.06	3.07	2.93	1.96	1.28	1.79	1.65	2.02	1.80
Nd	13.7	14.4	13.8	13.8	10.3	6.94	9.44	9.28	10.71	9.60
Sm	3.70	3.97	3.96	3.80	3.49	2.40	3.16	3.14	3.61	3.28
Eu	1.15	1.25	1.30	1.26	1.24	0.96	1.15	1.14	1.29	1.15
Gd	4.04	4.05	4.13	3.96	4.57	3.25	4.27	4.07	4.66	4.30
Tb	0.64	0.67	0.67	0.65	0.82	0.57	0.76	0.75	0.84	0.75
Dy	3.88	4.06	4.17	4.12	5.44	3.83	5.07	4.84	5.61	5.24
Ho	0.80	0.84	0.89	0.86	1.20	0.83	1.08	1.05	1.22	1.13
Er	2.29	2.37	2.43	2.44	3.59	2.50	3.32	3.09	3.66	3.40
Tm	0.32	0.34	0.34	0.35	0.52	0.37	0.48	0.48	0.54	0.49
Yb	2.15	2.27	2.14	2.34	3.51	2.46	3.24	2.95	3.63	3.33
Lu	0.32	0.32	0.31	0.34	0.52	0.36	0.48	0.46	0.54	0.50
Hf	2.38	2.43	2.33	2.42	2.38	1.49	2.21	1.95	2.54	2.30
Pb	5.00	5.28	4.71	5.00	3.90	2.41	3.43	3.70	3.87	3.43
Th*	1.270	1.38	1.13	1.15	0.220	0.418	0.335	0.304	0.351	0.324
U*	0.470	0.55	0.418	0.432	0.136	0.237	0.192	0.179	0.206	0.193
$^{87}Sr/^{86}Sr$	0.703433	0.703450	0.703435	0.703411	0.703469	0.703454	0.703479	0.703441	0.703475	0.703496
Error ± (2σ)	0.000034	0.000012	0.000013	0.000015	0.000015	0.000016	0.000013	0.000015	0.000014	0.000015
$^{143}Nd/^{144}Nd$	0.513046	0.513050	0.513041	0.513043	0.513093		0.513068	0.513077	0.513091	0.513111
Error ± (2σ)	0.000018	0.000008	0.000009	0.000006	0.000007		0.000013	0.000015	0.000008	0.000009
εNd	8.0	8.0	7.9	7.9	8.9		8.4	8.6	8.8	9.2
($^{238}U/^{232}Th$)	1.123	1.207	1.120	1.137	1.874	1.715	1.744	1.788	1.786	1.810
($^{230}Th/^{232}Th$)	1.067	1.148	1.097	1.048	1.413	1.350	1.377	1.364	1.389	1.390
Error ± (2σ)	0.018	0.009	0.005	0.002	0.006	0.006	0.006	0.017	0.017	0.020
($^{238}U/^{230}Th$)	1.052	1.051	1.022	1.086	1.326	1.271	1.267	1.311	1.285	1.302
Error ± (2σ)	0.024	0.009	0.006	0.004	0.008	0.008	0.008	0.018	0.018	0.029
($^{234}U/^{238}U$)	1.003		1.003	1.003	1.004		1.003	1.005		1.004
Error ± (2σ)	0.005		0.005	0.005	0.005		0.005	0.005		0.005

Table 1. (continued)

	Miyakejima									
	1962	1983-2903	1983-2808	1983-2908	2000-1	2000-2	2000-3	2000-4	2000-5	2000-A2
Eruption age	1962	1983	1983	1983	2000	2000	2000	2000	2000	2000
SiO_2(%)	56.78	53.30	53.31	54.75	53.13	52.7	53.08	52.22	52.29	54
TiO_2	1.27	1.38	1.38	1.35	1.36	1.17	1.35	1.26	1.26	1.37
Al_2O_3	14.81	15.09	15.19	15.04	14.74	17.91	14.75	16	15.95	14.84
FeO	11.60	13.36	13.16	12.43	13.58	11.37	13.63	12.83	12.86	13.1
MnO	0.23	0.24	0.24	0.23	0.26	0.21	0.26	0.24	0.24	0.24
MgO	3.46	4.02	4.09	3.84	4.5	3.6	4.46	4.35	4.37	4.02
CaO	7.83	9.17	9.22	8.72	9.39	10.33	9.41	10.2	10.11	8.88
Na_2O	3.13	2.75	2.71	2.87	2.43	2.25	2.44	2.35	2.36	2.83
K_2O	0.70	0.54	0.54	0.61	0.51	0.37	0.51	0.45	0.45	0.56
P_2O_5	0.17	0.15	0.15	0.16	0.12	0.09	0.12	0.11	0.11	0.16
Rb (ppm)	9.43	6.14	7.41	8.63	6.52	5.35	6.65	5.70	5.32	7.00
Sr	238	191	240	244	216	254	211	211	222	232
Zr	75.6	56.8	63.3	68.9	59.5	43.8	59.2	50.2	47.8	61.5
Nb	0.71	0.55	0.61	0.65	0.69	0.41	0.65	0.48	0.47	0.64
Cs	0.67		0.57	0.65		0.43				
Ba	251	166	203	224	175	160	172	149	155	195
La	4.22	3.19	3.51	3.98	3.25	2.66	3.42	3.11	2.94	3.70
Ce	12.5	9.07	10.5	11.7	9.13	7.92	9.65	8.73	8.42	10.5
Pr	2.07	1.60	1.75	1.91	1.59	1.36	1.68	1.56	1.46	1.77
Nd	10.78	8.54	8.93	10.15	8.75	7.63	8.83	8.35	7.93	9.62
Sm	3.62	3.02	3.11	3.35	2.95	2.72	3.28	2.95	2.79	3.29
Eu	1.24	1.15	1.13	1.18	1.10	1.10	1.13	1.11	1.08	1.28
Gd	4.65	4.34	4.08	4.36	4.29	3.64	3.95	3.92	3.87	4.47
Tb	0.83	0.82	0.73	0.77	0.78	0.64	0.77	0.74	0.70	0.82
Dy	5.69	4.99	4.89	5.36	4.96	4.45	4.97	4.88	4.52	5.40
Ho	1.22	1.11	1.07	1.16	1.07	0.96	1.10	1.06	0.97	1.12
Er	3.59	3.54	3.20	3.49	3.03	2.80	3.16	3.04	2.82	3.21
Tm	0.53	0.50	0.47	0.50	0.47	0.41	0.45	0.46	0.44	0.47
Yb	3.56	3.26	3.21	3.36	3.06	2.76	3.07	2.83	2.77	3.31
Lu	0.54	0.47	0.48	0.51	0.49	0.41	0.46	0.44	0.44	0.47
Hf	2.48	1.77	2.06	2.26	1.77	1.58	1.85	1.62	1.60	2.02
Pb	3.99	3.18	3.38	3.92	3.01	2.74	3.14	2.82	2.65	3.65
Th*	0.426	0.302	0.308	0.352	0.297	0.222	0.296	0.255	0.260	0.333
U*	0.250	0.180	0.186	0.211	0.170	0.136	0.170	0.154	0.155	0.197
$^{87}Sr/^{86}Sr$	0.703482	0.703518	0.703469	0.703512		0.703543	0.703517	0.703479	0.703531	0.703467
Error ± (2σ)	0.000014	0.000041	0.000024	0.000015		0.000018	0.000020	0.000023	0.000032	0.000024
$^{143}Nd/^{144}Nd$	0.513078	0.513070	0.513086	0.513080		0.513103	0.513067	0.513079	0.513074	0.513108
Error ± (2σ)	0.000010	0.000009	0.000007	0.000009		0.000007	0.000012	0.000027	0.000013	0.000009
εNd	8.6	8.4	8.7	8.6		9.1	8.4	8.6	8.5	9.2
($^{238}U/^{232}Th$)	1.781	1.807	1.827	1.814	1.734	1.853	1.740	1.837	1.813	1.801
($^{230}Th/^{232}Th$)	1.387	1.380	1.374	1.399	1.349	1.384	1.353	1.351	1.343	1.390
Error ± (2σ)	0.037	0.018	0.037	0.019	0.017	0.018	0.017	0.017	0.017	0.018
($^{238}U/^{230}Th$)	1.284	1.310	1.330	1.297	1.285	1.339	1.286	1.359	1.350	1.296
Error ± (2σ)	0.050	0.026	0.052	0.027	0.054	0.013	0.015	0.016	0.015	0.007
($^{234}U/^{238}U$)	1.000		0.992					1.006		
Error ± (2σ)	0.005		0.008					0.006		

Table 1. (continued)

	Miyakejima		Oshima					Niijima	Teishi Knoll
	2000-B1	2000-C1	JB2	Y3	Y5	Y1-Upper	Y1-Lower	Nij	TKN-102
Eruption age	2000	2000	1950–1951	1550 ± 5	1335 ± 10	1778	1778	2000–3000	1989
SiO_2(%)	53.9	54.00	53.07	52.58	52.186	52.49		51.46	49.70
TiO_2	1.37	1.355	1.17	1.29	1.30	1.29		1.19	0.82
Al_2O_3	14.93	14.93	14.49	13.78	13.62	13.91		16.119	16.48
FeO	13.05	12.99	14.30	15.02	14.95	14.69		13.61	10.14
MnO	0.24	0.24	0.22	0.22	0.22	0.22		0.23	0.17
MgO	4.01	4.06	4.60	4.76	4.77	4.65		4.61	7.70
CaO	8.97	8.89	9.77	9.50	9.48	9.60		9.80	11.03
Na_2O	2.82	2.85	1.98	1.82	1.90	1.937		2.52	2.06
K_2O	0.56	0.56	0.41	0.39	0.43	0.43		0.39	0.25
P_2O_5	0.15	0.16	0.10	0.10	0.10	0.10		0.13	0.12
Rb (ppm)	6.86	6.76	6.61	6.61	6.77	6.86	5.77	6.24	3.87
Sr	230	225	178	155	179	184	132	260	300
Zr	64.9	61.9	45.6	43.7	44.3	43.1	37.9	41.6	29.5
Nb	0.65	0.59	0.48	0.46	0.50	0.47	0.43	1.01	0.88
Cs			0.81		0.92	0.90		0.38	0.28
Ba	188	182	222	208	237	231	176	104	83.6
La	3.67	3.55	2.43	2.16	2.48	2.40	2.33	3.42	2.66
Ce	10.6	10.0	6.68	6.13	7.32	7.18	6.36	9.15	7.28
Pr	1.87	1.73	1.21	1.05	1.21	1.21	1.16	1.41	1.13
Nd	9.67	9.78	6.19	5.90	6.45	6.33	6.18	7.21	5.55
Sm	3.33	3.36	2.24	2.07	2.33	2.22	2.23	2.18	1.70
Eu	1.21	1.22	0.81	0.87	0.86	0.82	0.85	0.91	0.69
Gd	4.26	4.06	3.03	2.84	3.17	3.07	3.22	2.71	2.04
Tb	0.84	0.80	0.54	0.54	0.58	0.57	0.60	0.48	0.35
Dy	5.21	5.22	3.69	3.78	3.93	3.85	3.70	3.21	2.21
Ho	1.13	1.14	0.81	0.83	0.88	0.85	0.87	0.72	0.46
Er	3.32	3.30	2.44	2.49	2.61	2.59	2.45	2.04	1.36
Tm	0.53	0.50	0.36	0.40	0.38	0.38	0.38	0.30	0.19
Yb	3.36	3.20	2.42	2.41	2.69	2.57	2.55	2.05	1.32
Lu	0.50	0.48	0.36	0.38	0.39	0.37	0.41	0.30	0.19
Hf	2.03	1.97	1.42	1.53	1.56	1.47	1.44	1.32	0.93
Pb	3.52	3.38	5.37	5.45	4.25	4.17	3.71	2.22	1.56
Th*	0.332	0.317	0.28	0.272	0.269	0.266	0.270	0.415	0.244
U*	0.201	0.195	0.17	0.178	0.163	0.161	0.157	0.170	0.099
$^{87}Sr/^{86}Sr$	0.703591	0.703506	0.703657	0.703670	0.703735	0.703622	0.703649	0.703367	0.703303
Error ± (2σ)	0.000027	0.000028	0.000013	0.000013	0.000018	0.000012	0.000013	0.000015	0.000015
$^{143}Nd/^{144}Nd$	0.513072	0.513083	0.513103	0.513101	0.513089		0.513107	0.513064	0.513068
Error ± (2σ)	0.000013	0.000015	0.000006	0.000007	0.000008		0.000011	0.000011	0.000011
εNd	8.5	8.7	9.1	9.0	8.8		9.1	8.3	8.4
($^{238}U/^{232}Th$)	1.838	1.860	1.891	1.988	1.838	1.838	1.765	1.240	1.231
($^{230}Th/^{232}Th$)	1.406	1.444	1.219	1.276	1.295	1.224	1.258	1.125	1.157
Error ± (2σ)	0.018	0.018	0.016	0.011	0.002	0.029	0.030	0.011	0.007
($^{238}U/^{230}Th$)	1.307	1.288	1.552	1.558	1.420	1.502	1.402	1.134	1.095
Error ± (2σ)	0.021	0.021	0.056	0.025	0.006	0.057	0.053	0.027	0.014
($^{234}U/^{238}U$)	1.012	1.012	1.004	1.024			1.003	1.003	1.002
Error ± (2σ)	0.005	0.005	0.005	0.005			0.005	0.008	0.005

**U and Th abundances were determined by isotope dilution analyses.*

Table 2. Chemical compositions of plutonic rocks from the Tanzawa massif

Rock type	OTN5-1 Gabbro	MZ4-1 Tonalite	Y-1 Tonalite	OT5A-1 Tonalite
SiO_2(%)	43.15	63.08	69.68	56.86
TiO_2	1.34	0.57	0.39	0.48
Al_2O_3	19.74	17.21	15.15	20.07
FeO	12.82	5.50	3.87	6.73
MnO	0.18	0.13	0.11	0.17
MgO	7.17	2.39	1.66	3.57
CaO	14.04	6.43	4.78	8.22
Na_2O	1.45	3.81	3.73	3.61
K_2O	0.04	0.77	0.55	0.19
P_2O_5	0.06	0.11	0.08	0.12
Rb (ppm)	0.74	8.61	8.44	3.55
Sr	219	168	206	347
Zr	26.6	101	145	37.1
Nb	0.28	0.75	0.74	0.47
Ba	20.9	201	225	164
La	1.11	4.88	3.97	3.86
Ce	3.48	13.6	9.80	9.48
Pr	0.77	2.14	1.37	1.44
Nd	4.57	10.2	6.04	6.92
Sm	2.00	2.86	1.59	1.92
Eu	0.82	0.89	0.66	0.88
Gd	3.10	3.50	1.91	2.34
Tb	0.56	0.61	0.31	0.38
Dy	3.73	3.98	1.98	2.62
Ho	0.81	0.85	0.43	0.54
Er	2.27	2.58	1.34	1.69
Tm	0.32	0.42	0.22	0.25
Yb	1.95	2.68	1.51	1.67
Lu	0.28	0.43	0.26	0.26
Hf	0.78	2.58	3.08	0.91
Pb	0.69	2.53	2.65	3.18
Th*	0.074	1.21	0.72	0.20
U*	0.031	0.47	0.34	0.12
($^{238}U/^{232}Th$)	1.27	1.17	1.41	1.89

**U and Th abundances were determined by an ICP-MS with a quadrupole mass analyzer.*

Major element data for the samples from Miyakejima with eruption ages older than 2000 were published by Niihori *et al*. (2003). Major elements for other samples were analyzed using X-ray fluorescence spectrometry (XRF) at ERI (PW2400; Philips Japan Ltd.).

About 300 mg of samples were used for analyses of trace element abundances and isotopic compositions, including radioactive disequilibria. They were digested sequentially using $HF/HClO_4$ and HCl/H_3BO_3. Thorium fluoride, which might remain after $HF/HClO_4$ acid treatment, was dissolved using HCl/H_3BO_3 (Turner *et al*., 1997).

The concentrations of the trace elements except for U and Th were determined using an ICP-MS with a quadrupole mass analyzer (PQ3; Thermo Elemental, Winsford, UK). Accuracy and precision of the analyses are shown in Appendix 1. RSD of most of the elements was better than 10%. Acid digestion bombs (Parr) were used for decomposition of the samples of tonalite and gabbro from the Tanzawa plutonic complex. Aliquots of about 30-mg powder were used. Four days' digestion at 200°C in an oven decomposed almost all the samples. A few mineral grains, some of which appear to be zircon, remained in samples, except OTN5-1. However, because zirconium abundances showed no great difference from those obtained from XRF data (Tani, personal communication), it is unlikely that non-decomposed components greatly influence our trace element abundance data, at least aside from zirconium and hafnium.

The analytical scheme for ^{238}U–^{230}Th disequilibrium analysis was described in Fukuda and Nakai (2002). Uranium and thorium were purified using anion exchange resin (AGX1-8; Bio-Rad Laboratories Inc.). Abundance measurements were carried out using isotope dilution analysis. A reagent of depleted U ($U(NO_3)_4$, 94270; Fluka Chemika GmbH) was used as a U spike. The ^{230}Th spike was prepared by separation of ^{230}Th from natural U. The abundance and isotope measurements were performed using a MC-ICPMS (IsoProbe; GV Instruments Ltd., Manchester, UK). An Aridus micro-concentric nebulizer (Cetac Technologies) was used to introduce the sample solutions. The errors for the ($^{230}Th/^{232}Th$) and ($^{238}U/^{232}Th$) ratio were estimated respectively as about 0.5% and 2% (Fukuda and Nakai, 2002). About 200–300 mg of different batches of powdered samples were used for ($^{234}U/^{238}U$) analyses. After digestion, uranium was purified using a separation method with TRU-resin (TR-C50-A; Eichrom Technologies Inc.), as described by Pin and Zalduegui (1997). The precision of isotopic analyses depends on the amount of recovered uranium. It was around 5‰ when the uranium amount was around 10 ng, although it was about 2‰ when the uranium used for analyses was more than 20 ng.

Strontium and neodymium were purified using Sr-SPS resin (SR-B25-S, 50–100 mesh; Eichrom Technologies Inc.) and Ln resin (LN-B25-S, 50–100 mesh; Eichrom Technologies Inc.) following the method described by Nishio *et al*. (2004). The $^{87}Sr/^{86}Sr$ and $^{143}Nd/^{144}Nd$ data were normalized to $^{87}Sr/^{86}Sr = 0.710258$ for SRM987 and to $^{143}Nd/^{144}Nd = 0.5121067$ for JNdi-1. Before Sr isotopic measurements, we verified that peaks around m/e 83 (Kr) were less than the detection limit ($<10^{-4}$ A). Our $^{87}Sr/^{86}Sr$ and $^{143}Nd/^{144}Nd$ data for the standard rocks agree well with previously published data (Nishio *et al*., 2004).

RESULTS

Table 1 shows results of major and trace element analyses: Sr and Nd isotopic analyses and U–Th radioactive

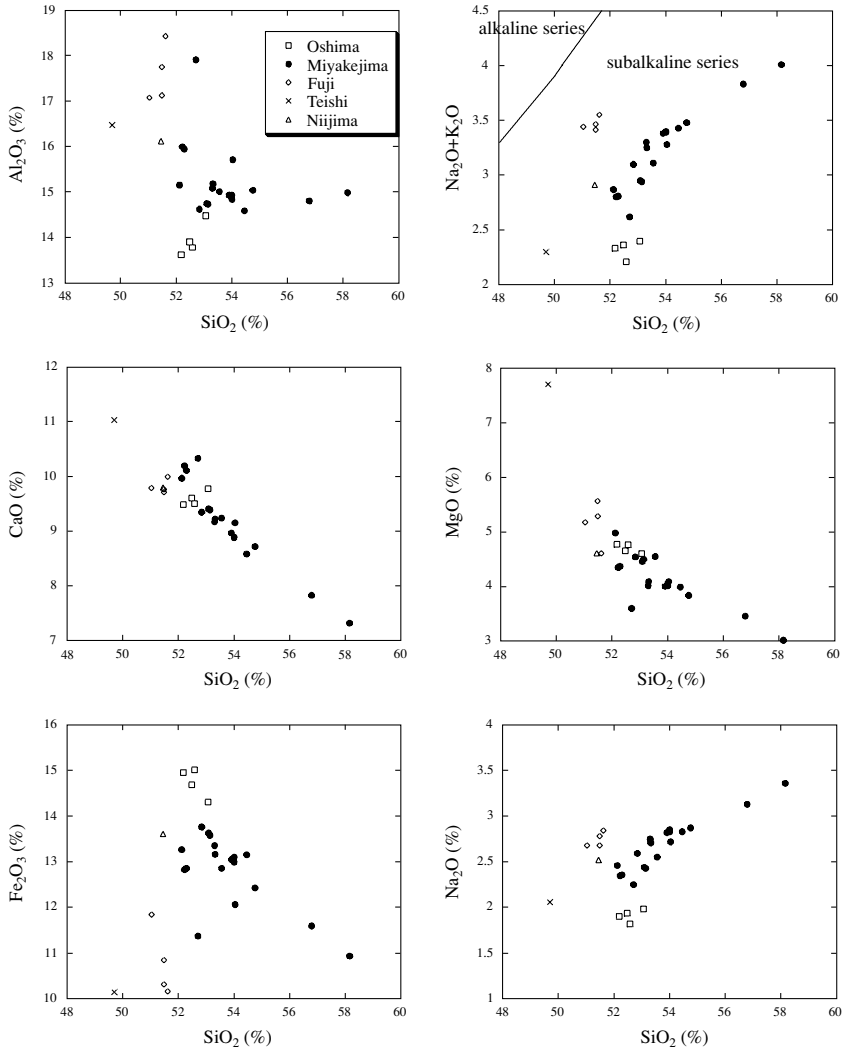

Fig. 2. Major elements abundance (as oxides) correlation diagrams of the samples from the Izu arc. The boundary between alkaline and subalkaline rocks on a total alkali vs. silica diagram is drawn following Kuno (1966).

disequilibrium analyses. The trace element abundance data of Tanzawa plutonic rocks are shown in Table 2.

Geochemistry of the samples

The samples' SiO_2 abundances were 49.7–58.2 wt%. The samples are classifiable into basalt to andesite using a $Na_2O + K_2O$ versus SiO_2 diagram (Fig. 2). Our results are consistent with those of previous studies (Takahashi *et al*., 1991; Watanabe *et al*., 2006; Kawanabe, 1991; Amma-Miyasaka and Nakagawa, 2003; Amma-Miyasaka *et al*., 2005; Koyaguchi, 1986; Yamamoto *et al*., 1991). Figure 2 shows correlation diagrams of SiO_2 with other major elements.

The N-MORB normalized trace element abundance patterns of the samples are shown in Fig. 3. The patterns show that the samples are rich in fluid mobile elements, such as Sr and Pb, and have apparently depleted HFSEs (Nb, Zr and Hf). The observed geochemical characteristics are common in volcanic rocks in subduction areas (e.g., Elliott *et al*., 1997; Yokoyama *et al*., 2003). Figure 4 shows chondrite-normalized REE patterns of the selected samples. The REE patterns of the samples from Oshima show slight light REE depletion, with flat patterns in the heavy REE. The variations of REE abundances are rather limited. The samples from Miyakejima show similar REE patterns to those from Oshima. However, the absolute REE abundances vary by a factor of 1.5. Some samples show a small positive or negative Eu anomaly. These observations on the samples of Miyakejima suggest that fractional crystallization played some role in trace element geochemistry. Phenocrysts of olivine and plagioclase have been reported for volcanic rocks from

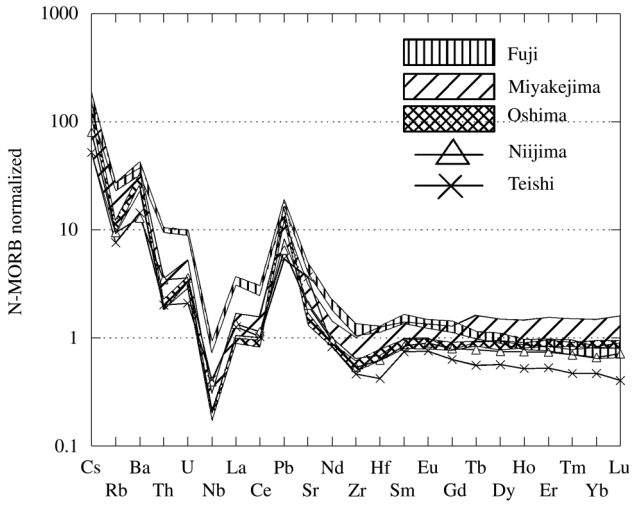

Fig. 3. Spider diagram normalized by N-MORB (Sun and McDonough, 1989) of the samples from the Izu arc.

the Miyakejima. The influence of fractional crystallization on the fractionation of trace elements will be discussed in Subsection "Influence of crystal fractionation". Among the samples from Miyakejima, REE patterns of samples with the lowest REE abundances overlap with those of Oshima. A sample from Niijima shows a flat REE pattern. The samples from Teishi Knoll and Fuji show slightly light REE enriched patterns and show a slightly positive Eu anomaly. No conspicuous negative Eu anomaly is observed in the analyzed samples except for the some samples from Miyakejima. Figure 4 shows that all samples except that from Teishi Knoll and differentiated ones from Miyakejima have similar HREE abundances. Larger variations observed in LREE and more incompatible elements might result from different degrees of melting and different degrees of mantle enrichment with slab-derived fluids or influences of previous depletion events. The samples from volcanoes with the shallowest depth to the Wadati-Benioff zone have lower concentrations of incompatible elements than those with deeper depth. The trend by which the abundances of incompatible elements increase with distance from the volcanic front has been commonly observed in other arcs as well. Kuno (1966) explained the cause of this trend as lesser degrees of melting behind the volcanic front. The across-arc variation will be discussed in Subsection "Across arc geochemical variation and regional mantle heterogeneity".

Isotopic compositions of the samples

Sr and Nd isotopic compositions Figure 5 shows $^{87}Sr/^{86}Sr$ and $^{143}Nd/^{144}Nd$ diagrams of the samples. The $^{87}Sr/^{86}Sr$ ratios of the samples from Miyakejima, Oshima, Teishi Knoll, Niijima, and Fuji are, respectively, 0.70344–

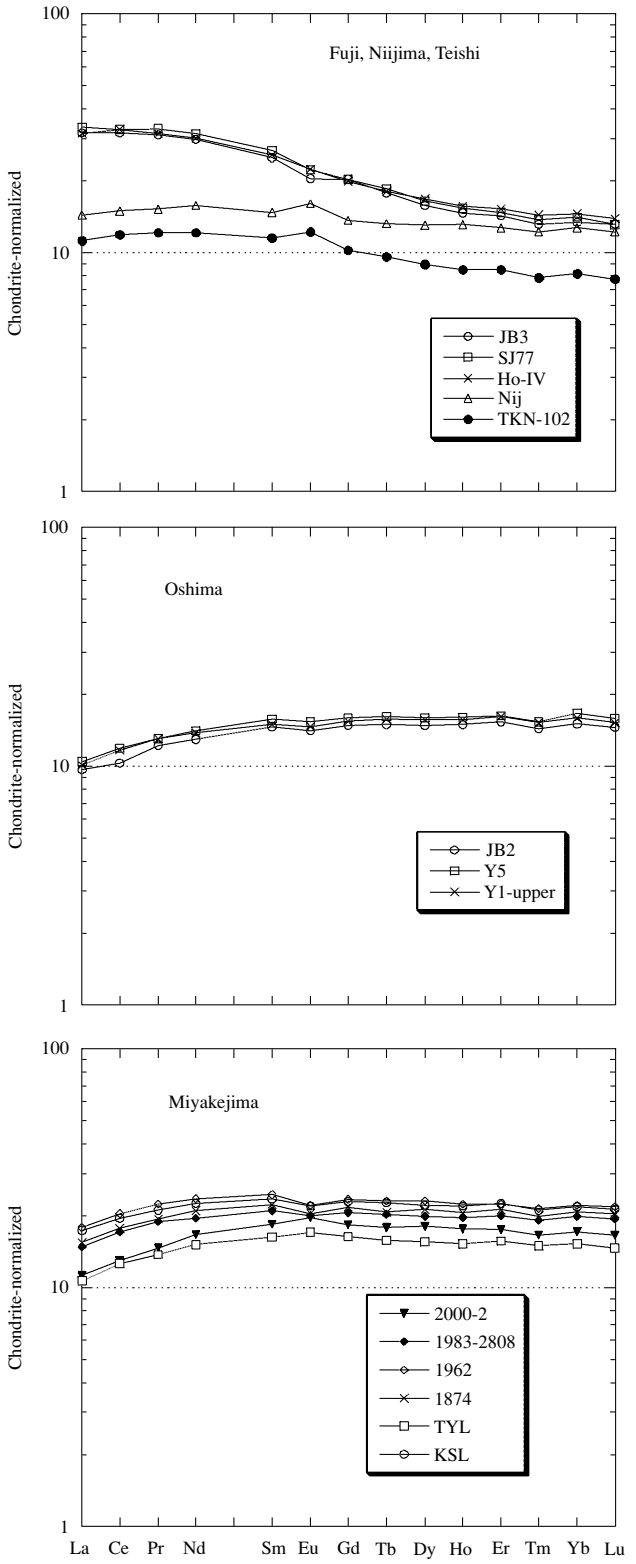

Fig. 4. Chondrite-normalized REE patterns of the samples from the Izu arc. In the top graph, JB3, SJ77 and Ho-IV are the samples from Fuji. Nij and TKN-102 are respectively from Niijima and Teishi Knoll.

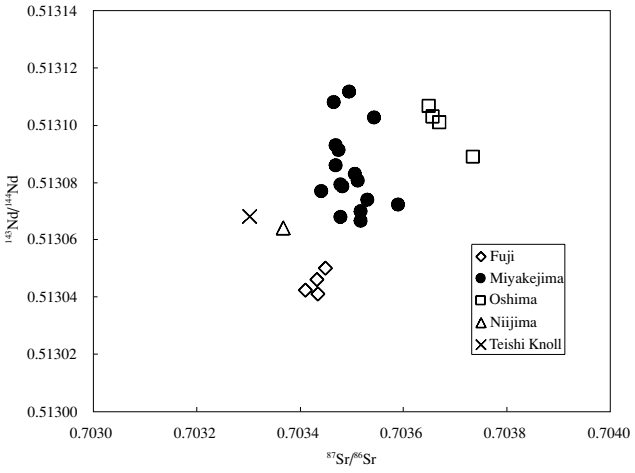

Fig. 5. ($^{86}Sr/^{87}Sr$) versus ($^{143}Nd/^{144}Nd$) diagram for Izu. Symbols have identical meanings to those in Fig. 2.

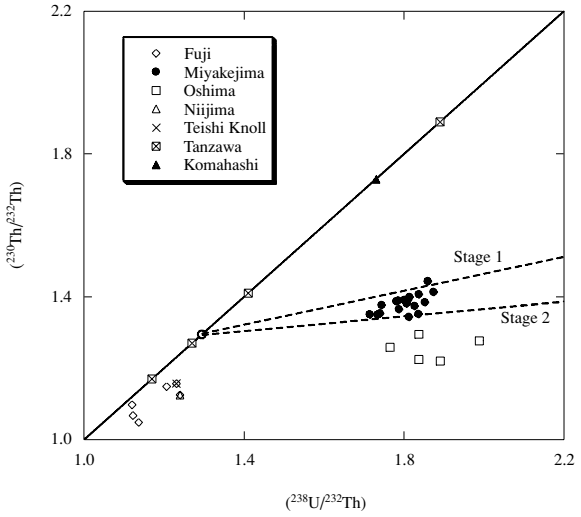

Fig. 6. A ($^{230}Th/^{232}Th$) versus ($^{238}U/^{232}Th$) diagram. The bold line is the equiline. Open circles on the equiline show the ($^{230}Th/^{232}Th$) value of the mantle beneath Miyakejima, as estimated by Yokoyama et al. (2003). The two dashed lines are regression lines for the samples of Stages 1 and 2 of Yokoyama et al. (2003). ($^{238}U/^{232}Th$) of the four samples of Tanzawa plutonic complex and the average of that of Komahashi-Daini Seamount are also shown assuming they attained radioactive equilibrium.

0.70359, 0.70362–0.70375, 0.70330, 0.70337 and 0.70341–0.70345. The $^{143}Nd/^{144}Nd$ ratios of the samples from Miyakejima, Oshima, Teishi Knoll, Niijima and Fuji are, 0.51307–0.51311, 0.51309–0.51311, 0.51307, 0.51306, and 0.51304–0.51305, respectively.

U–Th radioactive disequilibrium Figure 6 shows the U–Th equiline diagram. Yokoyama *et al*. (2003) analyzed the ^{238}U–^{230}Th–^{226}Ra disequilibria of the samples from Miyakejima in the northern Izu arc. They presented two regression lines in a ($^{230}Th/^{232}Th$)–($^{238}U/^{232}Th$) diagram: one for the samples of two older stages, whose eruption periods were between *ca*. 25–10 ka and 7000 years BP (Stage 1); and one for the samples between 7000 and 4000 BP (Stage 2). Using the intersection of the two lines and the equiline, Yokoyama *et al*. (2003) estimated ($^{230}Th/^{232}Th$) of the mantle beneath Miyakejima to be 1.30. The two regression lines and the ($^{230}Th/^{232}Th$) value are also shown in Fig. 6.

In the samples from the Izu arc, as in many other arc samples such as Mariana, Tonga–Kermadec and Chile arcs (Elliott *et al*., 1997; Turner *et al*., 1997; Sigmarsson *et al*., 1990), excess (^{238}U) relative to (^{230}Th) is apparent. In the ^{238}U–^{230}Th diagram (Fig. 6), the data for respective volcanoes are shown in different regions: ($^{238}U/^{232}Th$) and ($^{230}Th/^{232}Th$) are 1.82–2.05 and 1.22–1.30 at Oshima, and 1.77–1.93 and 1.35–1.44 at Miyakejima, respectively. Ratios of ($^{238}U/^{230}Th$) were 1.44–1.60 at Oshima and 1.30–1.40 at Miyakejima. In Fuji, Niijima and Teishi Knoll, their ($^{238}U/^{232}Th$) and ($^{230}Th/^{232}Th$) are 1.15–1.28 and 1.05–1.16, respectively. The values of ($^{238}U/^{230}Th$) were 1.02–1.13, which are smaller than those of Oshima and Miyakejima. The analyzed samples do not define a clear correlation line, as shown in the case of the Mariana (Elliott *et al*., 1997). Sigmarsson *et al*. (2006) analyzed U–Th–Ra and U–Pa radioactive disequilibria in arc lavas from the Izu arc and also reported that there was no correlation between ($^{238}U/^{232}Th$) and ($^{230}Th/^{232}Th$).

DISCUSSION

Across arc geochemical variation and regional mantle heterogeneity

In Fig. 7, Ba/Th, ($^{238}U/^{230}Th$), ($^{230}Th/^{232}Th$) and La/Yb are plotted against the depth to the Wadati-Benioff zone at each volcano.

($^{238}U/^{230}Th$) decreases in the order of Oshima, Miyakejima and the group of Niijima, Teishi Knoll and Fuji. The order is consistent with that of the depth to the Wadati-Benioff zone at each volcano, as shown in Fig. 7. Actually, ($^{238}U/^{230}Th$) correlates well with the Ba/Th ratio, as shown in Figs. 7(a) and (b). The observed across-arc variations in Ba/Th and ($^{238}U/^{230}Th$) reflect the difference in the degree of fluid addition, which decreases according to the depth to the Wadati-Benioff zone. Geochemical investigations of the Izu arc have revealed across-arc variation in the influence of a subducting slab component including components from both sediment and altered oceanic crust (AOC). Stable isotopic tracers of Li and B and radiogenic tracers of Sr, Nd and Pb indicate that slab-derived fluid, which contained two components from sediment and AOC, influenced isotopic composi-

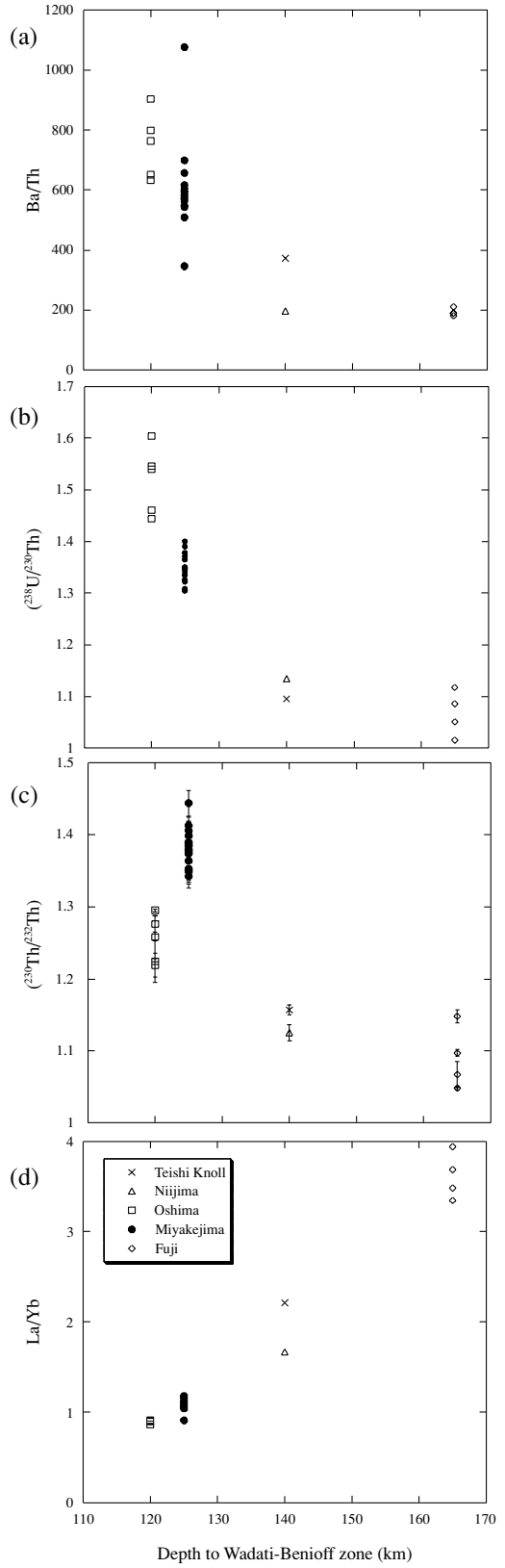

Fig. 7. Relationships between (a) Ba/Th, (b) ($^{238}U/^{230}Th$), (c) ($^{232}Th/^{230}Th$) and (d) La/Yb of the samples and the depth to the Wadati-Benioff zone at each volcano of the Izu arc.

tions of magmas (Ishikawa and Nakamura, 1994; Moriguti and Nakamura, 1998; Taylor and Nesbitt, 1998; Ishizuka *et al*., 2003, 2006). Although the relative importance of the sediment component to the AOC component is estimated differently by researchers for different isotopic systems, all agree that the influence of fluid addition is diminished in the back-arc side. The tendencies that are displayed in Figs. 7(a) and (b) are consistent with other isotopic systems described above. However, ($^{230}Th/^{232}Th$) of the samples from Miyakejima are higher than those from Oshima and the order of the two islands inverts, as shown in Fig. 7(c). Regional heterogeneity in ($^{230}Th/^{232}Th$) might pertain. Figure 7(d) shows La/Yb increases at the back-arc side. This trend reflects larger degrees of melting and more extensive depletion caused by previous melting events at the volcanic front.

Influences of crystal fractionation

We examine the possible influence of trace element fractionation in shallow crustal levels in this section. It has been recognized that processes, such as crystal fractionation and magma mixing, in shallow crustal levels modified chemical compositions of volcanic rocks (Watanabe *et al*., 2006; Kawanabe, 1991; Amma-Miyasaka and Nakagawa, 2003; Amma-Miyasaka *et al*., 2005; Koyaguchi, 1986). Major element correlation diagrams (Fig. 2) present the influence of fractional crystallization, as shown in the variation of SiO_2 (53–58%) content for the samples from Miyakejima. The presence of phenocrysts of olivine, plagioclase, clinopyroxene, orthopyroxene, and magnetite are reported in the samples. Figure 8 shows variations in trace elements concentrations in the samples analyzed in this study. While Sr/Th ratio (Fig. 8(a)) shows large variation, indicating the influence of crystal fractionation, other ratios including U/Th ratio show limited variation (less than 10%) among the lavas from individual islands (Figs. 8(b) and (c)). Although the crystal fractionation influences ^{238}U–^{230}Th disequilibrium to some extent, it will not influence the discussions in Subsections of "($^{238}U/^{232}Th$)–($^{230}Th/^{232}Th$) correlation of the samples from the Izu and the Mariana arcs" and "Isotopic variations in the Izu and Mariana arcs".

Influence of sea water alteration and weathering

We next examine the possible influence of trace element fractionation by seawater alteration and weathering. Samples of 2000-A2, 2000-B1, 2000-C1 from Miyakejima and TKN-102 from Teishi Knoll were collected from the seafloor. Seawater and groundwater are rich in U relative to Th: seawater and groundwater alteration can also influence ^{238}U–^{230}Th disequilibria (Yokoyama *et al*., 2003). Yokoyama *et al*. (2003) found that the abundance ratios of fluid mobile to fluid immo-

bile elements, such as Th/U and Nb/B, in basalt samples from Miyakejima correlated with the ($^{234}U/^{238}U$) activity ratio. The correlation lines connecting seawater points with ($^{234}U/^{238}U$) of 1.14 and non-altered basalts with ($^{234}U/^{238}U$) of unity in ($^{234}U/^{238}U$) versus Th/U and Nb/B diagrams were interpreted by the authors as mixing lines (Yokoyama *et al*., 2003). Therefore, the ($^{234}U/^{238}U$) activity ratio can be used as an indicator of seawater alteration. We analyzed ($^{234}U/^{238}U$) of 17 samples. The values of ($^{234}U/^{238}U$) of fourteen samples used for ^{238}U–^{230}Th analyses in this study are unity, within analytical error; it is unlikely that seawater alteration markedly influenced ^{238}U–^{230}Th disequilibria for these samples. Two samples from Miyakejima, 2000-B1, 2000-C1, collected from the sea floor show (^{234}U) enrichment relative to (^{238}U), indicating the influence of seawater alteration. One sample from Ohima, Y3, although collected at the caldera rim at 500m elevation, shows disequilibrium between (^{234}U) and (^{238}U). This sample might have been altered by surface weathering. The ($^{238}U/^{232}Th$) values of the altered samples are higher relative to those of unaltered samples from the same volcano and they might have been increased by about 10–20% by alteration. A correlation diagram between (Nb/U)–($^{234}U/^{238}U$) (not shown) shows no clear correlation. We recognize the influence of alteration in some samples, however, the discussion in Subsections of "($^{238}U/^{232}Th$)–($^{230}Th/^{232}Th$) correlation of the samples from the Izu and the Mariana arcs" and "Isotopic variations in the Izu and Mariana arcs" will hold with the data of the samples without ($^{234}U/^{238}U$) disequilibria.

Influence of crustal contamination

In the ^{238}U–^{230}Th diagram (Fig. 6), the points of respective volcanoes are shown in different regions. Yokoyama *et al*. (2003) estimated ($^{230}Th/^{232}Th$) of the mantle beneath Miyakejima at 1.30 from the intersection of two regression lines drawn for the two stages of the samples from the volcano; also, the regression lines and the thorium isotopic composition of the mantle are shown in Fig. 6. The estimated initial mantle value is much higher than those of Fuji, Niijima, and Teishi Knoll.

In Fig. 6, the points for Fuji, Niijima, and Teishi Knoll are shown in the region where both ($^{238}U/^{232}Th$) and ($^{230}Th/^{232}Th$) are less than 1.3. This disequilibrium diagram might indicate difference in U/Th abundance ratio and Th isotopic composition, within the Izu arc. Alternatively, the magmas of the samples have undergone crustal contamination to various degrees, as indicated by the fact that crustal materials often have low U/Th ratios. We discuss the possible influence of crustal contamination in this section.

Results of a marine seismic reflection and ocean bottom seismographic refraction survey suggested the presence of a middle crust with granitic composition in the

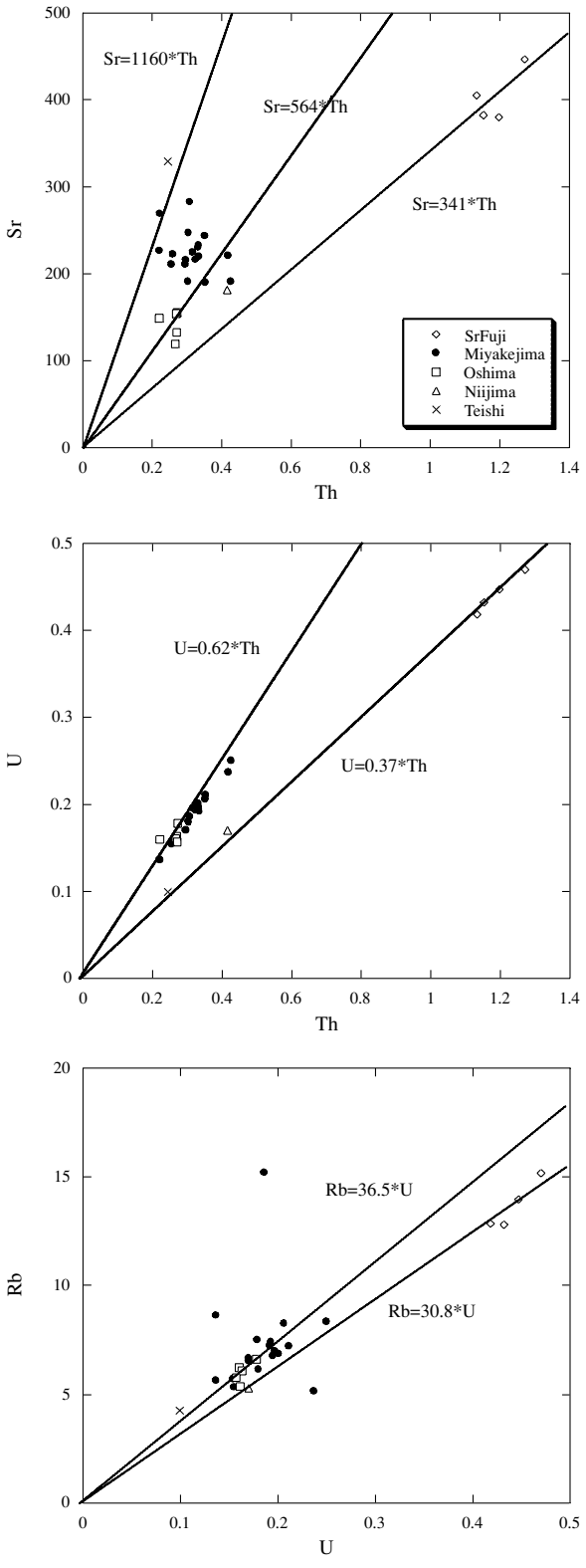

Fig. 8. (a) Sr versus Th, (b) U versus Th, (c) Rb versus U concentrations (μg/g) for the samples analyzed in this study.

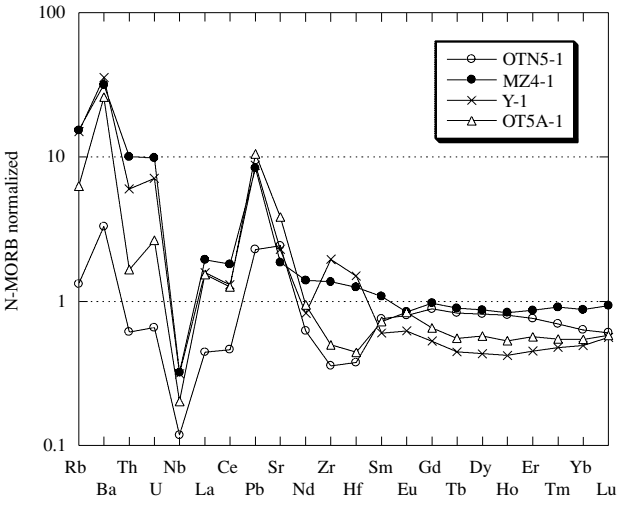

Fig. 9. N-MORB-normalized spider diagram of the plutonic rocks from the Tanzawa area.

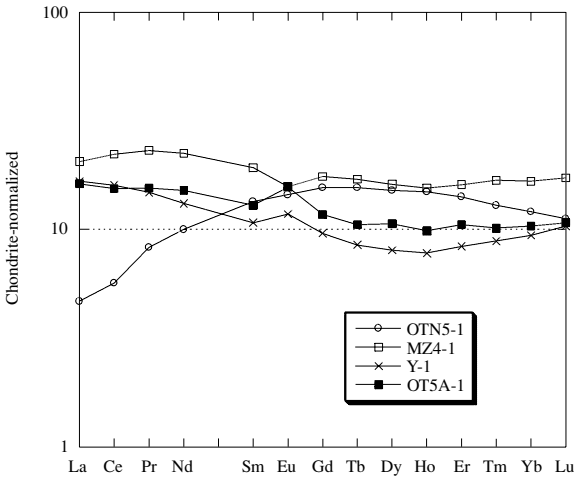

Fig. 10. Chondrite-normalized REE patterns of the plutonic rocks from the Tanzawa area.

Izu oceanic island arc (Suyehiro *et al*., 1996; Takahashi *et al*., 1998; Kodaira *et al*., 2007). The variability of the granitic layer thickness might cause various degrees of crustal contamination, which can engender variation in the (^{230}Th/^{232}Th) ratios of the samples if the granitic layer has significantly different (^{230}Th/^{232}Th) and (^{238}U/^{232}Th) ratios from the volcanic rocks.

A plutonic complex exposed in the Tanzawa area, north of the Izu arc (Fig. 1), consisting mainly of tonalite, has been considered to represent the lower-middle crust of the Izu arc (Ishizaka and Yanagi, 1977; Kawate and Arima, 1998; Taira *et al*., 1998). Few data have been reported for uranium and thorium. The results of trace element abundances of samples of the Tanzawa plutonic complex are shown in Table 2 and Figs. 9 and 10. A spider diagram of the samples from the Tanzawa area shows a large Nb negative anomaly and large positive anomaly in Pb and Sr. Those features suggest that the Tanzawa plutonic complex shares geochemical signatures of island-arc volcanic rocks. The (^{238}U/^{232}Th) ratios of the samples of plutonic complex, as shown in Fig. 6, vary within 1.2–2.0, which are higher than those of the samples from Fuji, Niijima, and Teishi Knoll but similar to or higher than those of Miyakejima. The Th abundances of the plutonic rocks ranges from 0.074 to 1.2 ppm. Two samples with high Th abundance have (^{230}Th/^{232}Th) similar to those of volcanic rocks analyzed in this study.

Geochemical data related to tonalitic rocks dredged from the Komahashi-Daini Seamount in the northern Kyushu–Palau Ridge, which can be also a candidate for the assimilated crustal material, have been reported by Haraguchi *et al*. (2003). The tonalities are part of an intrusive body of tonalitic middle crust generated in the older Izu-Ogasawara (Bonin)–Mariana (IBM) arc. Their Th abundances and (^{238}U/^{232}Th) were 0.36–1.01 ppm and 1.17–2.94, respectively, with averages of 0.67 ± 0.19 and 1.71 ± 0.50 (1σ, n = 9). As stated above, the data from the Tanzawa plutonic complex and Komahashi-Daini Seamount indicate that the abundances of U and Th in crustal material in this area are not significantly higher than those of volcanic rocks analyzed in this study. Therefore, it is unlikely that the ^{238}U–^{230}Th disequilibrium system of the volcanic rocks analyzed in this study has been modified substantially unless significant assimilation of crustal material (more than 10%) happened. Major element data of the volcanic rocks are inconsistent with significant crustal assimilation.

(^{238}U/^{232}Th)–(^{230}Th/^{232}Th) correlation of the samples from the Izu and the Mariana arcs

Figure 6 apparently suggests that the analyzed samples from Izu arc do not define a clear correlation line, as shown in the case of the Mariana (Elliott *et al*., 1997). However, plotting the current data with those from the Mariana arc reveals that most of the samples from the two arcs form a well-defined correlation line in the isochron diagram except the samples from Miyake-jima and Alamagan (Fig. 11). Data from the Kasuga seamount (Gill and Williams, 1990) obtained by α spectrometry also plot on the line. If we interpret this correlation line as an isochron, the slope of the line gives an age of around 24 ka. The correlation line suggests the presence of a common end-member in low (^{238}U/^{232}Th) side. It is likely that the wedge mantle beneath the two arcs share a common Th radioactivity ratio with the exceptions of Miyake-jima and Alamagan. The (^{230}Th/^{232}Th) at the intersection between the correlation line and the equiline is around 1.05 ± 0.05.

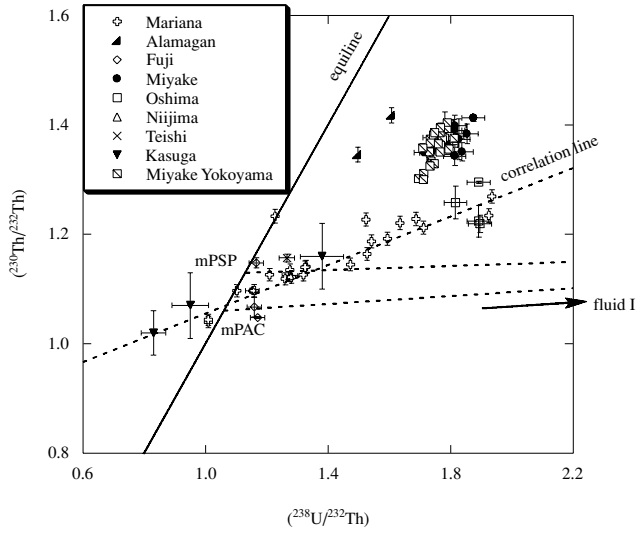

Fig. 11. Equiline plot of Izu and Mariana samples. Data of Miyakejima (Yokoyama et al., 2003), Mariana (Elliott et al., 1997) and Kasuga seamount (Gill and Williams, 1990) are plotted together with those obtained in this study. The samples with ($^{234}U/^{238}U$) different from unity are not plotted. Correlation line is regressed (Ludwig, 2001) through data points of Kasuga seamount and Mariana except Alamagan and those of Izu except Miyakejima. Two mixing lines between modified PSP and fluid I and between modified PAC and fluid I (see Appendix 2) are also shown.

In the same figure, there are two mixing lines between two mantle components: modified source for Philippine Sea Plate MORB (mPSP hereafter) and modified source for Pacific MORB (mPAC hereafter), and a fluid equilibrated with the mixture of altered oceanic crust (AOC) and sediment, fluid I. The compositions of the fluid I are calculated by assuming 2% fluid equilibrated with a mixture of AOC and sediment with a proportion of 0.98:0.02 and fluid/rock distribution coefficients reported by Brenan *et al*. (1995). The compositions of the two mantle components were estimated following the discussion in the next section. The compositions of the mantle and fluid end-members are described in Appendix 2 in detail. The two mixing lines show the relationship between ($^{238}U/^{232}Th$) and ($^{230}Th/^{232}Th$) at the time of fluid addition. Then, if the above mantle-fluid mixing model is correct, the magma sources should distribute around the mixing lines, whose slopes correspond to ages of around 6 and 8 ka for the mPAC-fluid I and mPSP-fluid I, respectively. The time lag between fluid addition and eruption can be calculated from the difference in the slope of the observed correlation line and that of the mixing line and it would be less than 20 kyr. The slope of the mixing line, however, depends on distribution coefficients of Th and U between fluid and minerals and quantitative interpretation is difficult.

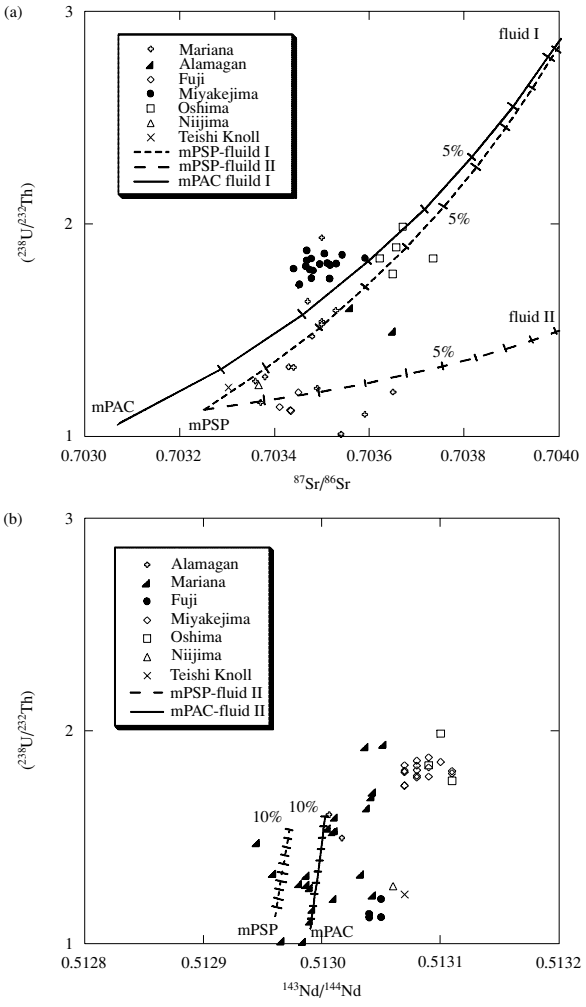

Fig. 12. ($^{238}U/^{232}Th$) versus (a) $^{87}Sr/^{86}Sr$ and (b) $^{143}Nd/^{144}Nd$ diagram for samples from the Izu arc analyzed in this study and those for the samples from Mariana arc (Elliott, 1997). Mixing curves between two mantle components (mPSP and mPAC) and two types of fluids (fluid I and fluid II) are also shown. Chemical compositions of the mantle components and the fluids used for the mixing calculation are described in Appendix 2. Chemical compositions of the fluid I and fluid II are calculated assuming that they are equilibrated with mixture of AOC and sediment components with a proportion of 0.98:0.02 by distribution coefficients reported by Brenan et al. (1995) and Kessel et al. (2005), respectively. The tick marks on the curves represent the percentage of fluid addition.

Isotopic variations in the Izu and Mariana arcs

While initial ($^{230}Th/^{232}Th$) before the last fluid addition is relatively homogeneous, the samples from the two arcs hold relatively larger variation in Sr and Nd isotopic ratios. Taylor and Nesbitt (1998) reported considerable along-arc variation in Sr, Nd and Pb isotopes in the Izu arc. Ishizuka *et al*. (2003, 2006) identified an along-arc isotopic variation of lavas both in the volcanic front of

the arc and in the back-arc region of the Izu arc.

Here we consider how the mantle beneath the Izu and Mariana arcs can be homogeneous regarding Th radioactivity ratio in spite of considerable variation in Sr and Nd isotopic ratios. Figure 12 show the correlation of (^{238}U/^{232}Th) versus ^{87}Sr/^{86}Sr and ^{143}Nd/^{144}Nd of the samples analyzed in this study, with results of model calculation to infer the influence of fluid components. (^{238}U/^{232}Th) is used in place of (^{230}Th/^{232}Th) in the plots because 1) influence of in-growth should be considered when (^{230}Th/^{232}Th) is used, 2) large elemental fractionation between U and Th is unlikely in magma evolution processes.

In Fig. 12(a), two mixing curves starting from the modified PSP mantle show the results of addition of fluid I and fluid II. The compositions of the fluid II are calculated by assuming 2% fluid equilibrated with mixture of AOC and sediment with a proportion of 0.98:0.02 using distribution coefficients reported by Kessel *et al*. (2005). Variation of the proportion of the sediment component (0–5%) does not modify the shape of the curves so much (not shown). The distribution coefficients give more influences on the slope of the curve. The model curve calculated with Kessel's partition coefficients has a gentler slope. A mixing curve between the modified PAC mantle and fluid I is also shown. Parameters used in the calculation of fluid compositions and the compositions of two-types of subarc mantle sources chosen for the mixing calculations are described in Appendix 2. Many samples from the two arcs plot near the mixing curves calculated with Brenan's distribution coefficients, suggesting that isotopic variation in Sr can be mostly explained by fluid addition. In Fig. 12(a), the data points of Miyakejima and Oshima are located in the high (^{238}U/^{232}Th) and high ^{87}Sr/^{86}Sr areas, which is consistent with the view that these islands with shallower depth to the Wadati-Benioff zone have been metasomatized by a fluid component more than the volcanoes with deeper depth. The tendencies that are displayed in Fig. 12(a) are consistent with other isotopic systems described in Subsection "Across arc geochemical variation and regional mantle heterogeneity".

In Fig. 12(b), two curves show addition of the fluid II to the modified PSP and the modified PAC mantle. Because Brenan *et al*. (1995) did not report the distribution coefficient for Nd, we used the set of the coefficients reported in Kessel *et al*. (2005). Figure 12(b) shows that addition of fluid cannot greatly modify ^{143}Nd/^{144}Nd. A process other than fluid addition is required to produce the observed variation in Nd isotopic ratios.

Figure 13(a) shows a relationship between chondrite-normalized (La/Nd) and ^{143}Nd/^{144}Nd. The samples from the two arcs show a linear correlation. The original mantle should lie on the right hand side of the array, while the sediment-derived component is probably the left hand end-member. Figure 13(b) shows a relationship between

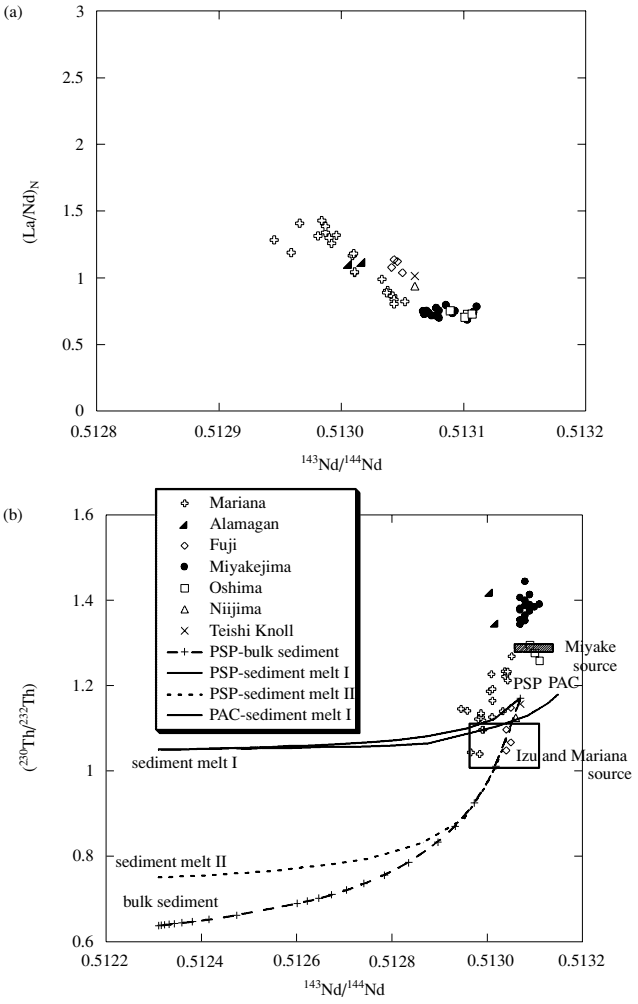

Fig. 13. (a) ^{143}Nd/^{144}Nd versus (La/Nd)$_N$ (chondrite-normalized abundance ratio) and (b) ^{143}Nd/^{144}Nd versus (^{230}Th/^{232}Th) of the Izu samples. In (b), three mixing curves between PSP mantle and bulk sediment, sediment melt I, sediment melt II and one mixing curve between PAC mantle and sediment melt I are shown. Source composition before the last fluid addition for Mariana and Izu volcanoes except Miyakejima and Alamagan, and that for Miyakejima are shown in a transparent and a shaded horizontal rectangle, respectively.

^{143}Nd/^{144}Nd and (^{230}Th/^{232}Th) of the source materials of the volcanic rocks from Izu and Mariana together with those of the volcanic rocks. Mixing curves between mantle components and sediment-derived components, bulk sediment and two types of aged sediment melt, are also shown. The sources of Philippine Sea Plate MORB (PSP hereafter) and Pacific MORB (PAC hereafter) are used as mantle end-members following Ishizuka *et al*. (2003). Regarding another end-member, Elliott *et al*. (1997) concluded that addition of sediment component via sediment melt not bulk sediment dominates incompatible element

budgets of the lavas from the Mariana arc and it can explain high abundance ratios of incompatible elements/high strength field elements in the lavas. Tollstrup and Gill (2005) also concluded that a partial melt of subducted metasediment saturated with accessory phases is required to reproduce the Nd–Hf isotopic systematics of the Mariana arc. In Fig. 13(b), a bold curve shows a mixing curve between PSP mantle and a 25% non-modal batch melt of bulk sediment of ODP1149 (sediment melt I). A mixing curve between PAC mantle and sediment melt I is also shown. Parameters used in the calculation are described in Appendix 2. The sediment melt I is equilibrated with cpx, garnet and accessory phases of rutile, zirocon and monazite. Mixing of the sediment melt I with the PSP mantle or the PAC mantle can reproduce homogeneous (^{230}Th/^{232}Th) at around 1.1 with variation in ^{143}Nd/^{144}Nd. The model calculation shows a possible mechanism, although it is not certain if the mode composition of trace accessory phases, which determine a melt composition, is homogeneous through the Izu and the Mariana arcs. Neither addition of bulk sediment nor sediment melt equilibrated with only cpx and garnet (sediment melt II) can reproduce the observed (^{230}Th/^{232}Th). In Fig. 12(a), some samples plot off the mixing curves to the higher ^{87}Sr/^{86}Sr side. The deviations from the mixing curves may be partly attributable to the influence of sediment melt addition, although it cannot explain the whole spectrum of ^{87}Sr/^{86}Sr.

The Miyakejima and Alamagan samples show significantly higher (^{230}Th/^{232}Th) than the array defined by the other samples in Fig. 11. Because trace element abundance ratios between a fluid mobile/an immobile element such as Ba/Th and (^{238}U/^{230}Th) of the samples from Miyakejima define a depth-dependent variation trend with the samples from other islands, it is unlikely that the influence of fluid addition to the magma source of the island significantly surpasses those to other islands. Therefore, we ascribe the higher (^{230}Th/^{232}Th) of the Miyakejima to sediment melt with higher (^{230}Th/^{232}Th).

Conclusions

The results of ^{238}U–^{230}Th disequilibrium analyses of lava samples from the Izu arc indicate ^{238}U excesses relative to ^{230}Th, which were commonly observed in many other arc systems such as those of the Mariana and the Tonga–Kermadec arcs. While across-arc variation is evident in degrees of (^{238}U) excess relative to (^{232}Th), the samples from Miyakejima deviate an across-arc variation trend in (^{230}Th/^{232}Th). The combined data of (^{230}Th/^{232}Th)–(^{238}U/^{232}Th) of the samples from the Izu and the Mariana arc revealed a well defined array in an equiline diagram with the exceptions of the samples from Miyakejima and Alamagan. The contribution from sediment melt dominated the Th budget in the sub-arc mantle and homogenized (^{230}Th/^{232}Th). The fact that many volcanoes with different depths to the Wadati-Benioff zone share the common (^{230}Th/^{232}Th) requires that influence of fluid addition had not accumulated to modify Th activity ratio before the final fluid addition.

Acknowledgments—This research was partly supported by grants-in-aid for scientific research to SN from Ministry of Education, Culture, Sports, Science and Technology. We are grateful to K. Kato for assistance with laboratory maintenance. We are indebted to J. B. Gill and an anonymous reviewer for their helpful comments and constructive criticism that greatly contributed to improving the manuscript.

References

Amma-Miyasaka, M. and Nakagawa, M. (2003) Evolution of deeper basaltic and shallower andesitic magmas during the AD 1469–1983 eruptions of Miyake-Jima volcano, Izu–Mariana arc: Inferences from temporal variations of mineral compositions in crystal-clots. *J. Petrol.* **44**, 2113–2138.

Amma-Miyasaka, M., Nakagawa, M. and Nakada, S. (2005) Magma plumbing system of the 2000 eruption of Miyakejima Volcano, Japan. *Bull. Volcan.* **67**, 254–267.

Bea, F., Pereira, M. D. and Stroh, A. (1994) Mineral/leucosome trace-element partitioning in a peraluminous migmatite (a laser ablation-ICP-MS study). *Chem. Geol.* **117**, 291–312.

Bedard, J. H. (1999) Petrogenesis of Boninites from the Betts Cove Ophiolite, Newfoundland, Canada: Identification of subducted source components. *J. Petrol.* **40**, 1853–1889.

Blundy, J. and Wood, B. (2003) Mineral-melt partitioning of uranium, thorium and their daughters. *Rev. Mineral. Geochem.* **52**, 59–123.

Brenan, J. M., Shaw, H. F., Ryerson, F. J. and Phinney, D. L. (1995) Mineral-aqueous fluid partitioning of trace elements at 900°C and 2.0 GPa: constraints on the trace element chemistry of mantle and deep crustal fluids. *Geochim. Cosmochim. Acta* **59**, 3331–3350.

Elliott, T., Plank, T., Zindler, A., White, W. and Bourdon, B. (1997) Element transport from slab to volcanic front at the Mariana arc. *J. Geophys. Res.* **102**, 14991–15019.

Fukuda, S. and Nakai, S. (2002) ^{238}U/^{230}Th disequilibrium measurement for volcanic standard rock samples using a multiple-collector ICPMS. *Geochem. J.* **36**, 465–473.

George, R., Turner, S., Hawkesworth, C., Bacon, C. R., Nye, C., Stelling, P. and Dreher, S. (2004) Chemical versus temporal controls on the evolution of tholeiitic and calc-alkaline magmas at two volcanoes in the Alaska–Aleutian arc. *J. Petrol.* **45**, 203–219.

Gill, J. B. and Williams, R. W. (1990) Th isotope and U–series studies of subductiou-related volcanic rocks. *Geochim. Cosmochim. Acta* **54**, 1427–1442.

Hamuro, K. (1985) Petrology of the Higashi-Izu monogenetic volcano group. *Bull. Earthquake Res. Inst. Univ. of Tokyo* **60**, 335–400.

Haraguchi, S., Ishii, T. and Kimura, J. (2003) Formation of tonalite from basaltic magma at the Komahashi-Daini seamount, northern Kyushu–Palau ridge in the Philippine Sea, and growth of the Izu-Ogasawara (Bonin)–Mariana arc

crust. *Contrib. Mineral. Petrol.* **145**, 151–168.
Hauff, F., Hoernle, K. and Schmidt, A. (2003) Sr–Nd–Pb composition of Mesozoic Pacific oceanic crust (Site 1149 and 801, ODP Leg 185): Implications for alteration of oceanic crust and the input into Izu-Bonin–Mariana subduction system. *Geochem. Geophys. Geosyst.* **4**, 8913, doi:10.1029/2002GC000421.
Hawkesworth, C., George, R., Turner, S. and Zellmer, G. (2004) Time scales of magmatic processes. *Earth Planet. Sci. Lett.* **218**, 1–16.
Hickey-Vargas, R. (1991) Isotope characteristics of submarine lavas from the Philippine Sea: implications for the origin of arc and basin magmas of Philippine tectonic plate. *Earth Planet. Sci. Lett.* **107**, 290–304.
Hickey-Vargas, R. (1998) Origin of the Indian Ocean-type isotopic signatures in basalts from Philippine Sea Plate spreading centers: an assessment of local versus large-scale processes. *J. Geophys. Res.* **103**, 20963–20979.
Hochstaedter, A. G., Gill, J. B., Taylor, B., Ishizuka, O., Yuasa, M. and Morita, S. (2000) Across-arc geochemical trends in the Izu-Bonin arc: Constraints on source composition and mantle melting. *J. Geophys. Res.* **105**, 495–512.
Hochstaedter, A. G., Gill, J. B., Peters, R., Broughton, P. and Holden, P. (2001) Across-arc geochemical trends in the Izu-Bonin arc: Contributions from the subducting slab. *Geochem. Geophys. Geosyst.* **2**, paper number 2000GC000105.
Imai, N., Terashima, S., Itoh, S. and Ando, A. (1995) 1994 Compilation of analytical data for minor and trace elements in seventeen GSJ geochemical reference samples, "igneous rock series". *Geostand. Geoanal. Res.* **19**, 135–213.
Ishikawa, T. and Nakamura, E. (1994) Origin of the slab component in arc lavas from across-arc variation of B and Pb isotopes. *Nature* **370**, 205–208.
Ishizaka, K. and Yanagi, T. (1977) K, Rb and Sr abundances and Sr isotopic composition of the Tanzawa granitic and associated gabbroic rocks, Japan: Low-potash island-arc plutonic complex. *Earth Planet. Sci. Lett.* **33**, 345–3512.
Ishizuka, O., Taylor, R. N., Milton, J. A. and Nesbitt, R. W. (2003) Fluid-mantle interaction in an intra-oceanic arc: constraint from high-precision Pb isotopes. *Earth Planet. Sci. Lett.* **211**, 221–236.
Ishizuka, O., Taylor, R. N., Milton, J. A., Nesbitt, R. W., Yuasa, M. and Sakamoto, I. (2006) Variation in the mantle sources of the northern Izu arc with time and space—Constraints from high-precision Pb isotopes. *J. Volcanol. Geotherm. Res.*, **156**, 266–290.
Isshiki, N. (1987) Geology of the Nii Jima district. *Quadrangle Series, Hachijojima (9) No. 1 (Guidebook.)*, Geological Survey of Japan (in Japanese with English abstract).
Jicha, B. R., Singer, B. S., Beard, B. L. and Johnson, C. M. (2005) Contrasting timescales of crystallization and magma storage beneath the Aleutian Island arc. *Earth Planet. Sci. Lett.* **236**, 195–210.
Kaneko, T., Yasuda, A., Shimano, T., Nakada, S., Fujii, T., Kanazawa, T., Nishizawa, A. and Matusmoto, Y. (2005) Submarine flank eruption preceding caldera subsidence during the 2000 eruption of Miyakejima Volcano, Japan. *Bull. Volcan.* **67**, 243–253.
Kawanabe, Y. (1991) Petrological evolution of Izu Oshima volcano. *Bull. Volcanol. Soc. Japan* **36**, 297–310 (in Japanese with English abstract).
Kawate, S. and Arima, M. (1998) Petrogenesis of the Tanzawa plutonic complex, central Japan: Exposed felsic middle crust of the Izu-Bonin–Mariana arc. *The Island Arc* **7**, 342–358.
Kelley, K. A., Plank, T., Ludden, J. and Staudigel, H. (2003) Composition of altered oceanic crust at ODP Sites 801 and 1149. *Geochem. Geophys. Geosyst.* **4**, 8910, doi:10.1029/2002GC000435.
Kessel, R., Schmidt, M. W., Ulmer, P. and Pettke, T. (2005) Trace element signature of subduction-zone fluids, melts and supercritical liquids at 120–180 km depth. *Nature* **437**, 724–727.
Kodaira, S., Sato, T., Takahashi, N., Ito, A., Tamura, Y., Tatsumi, Y. and Kaneda, Y. (2007) Seismological evidence for variable growth of crust along the Izu intraoceanic arc. *J. Geophys. Res.* **112**, B05104, doi:10.1029/2006JB004593.
Koyaguchi, T. (1986) Evidence for two-stage mixing in magmatic inclusions and rhyolitic lava domes on Niijima island, Japan. *J. Volcanol. Geotherm. Res.* **29**, 71–98.
Kuno, H. (1966) Lateral variation of basalt magma types across continental margins and island arcs. *Bull. Volcan.* **29**, 195–222.
Ludwig, R. K. (2001) User manual for Isoplot/Ex rev. 2.49. Berkeley Geochronology Center Special Publication 1a. Berkeley Geochronology Center, Berkeley, CA, 55 pp.
Machida, S. and Ishii, T. (2003) Backarc volcanism along the en echelon seamounts: The Enpo seamount chain in the northern Izu-Ogasawara arc. *Geochem. Geophys. Geosyst.* **4**, 9006, doi:10.1029/2003GC000554.
Mahoney, J. J., Sinton, J. M., Kurz, M. D., Mcdougall, J. D., Spencer, K. J. and Lugmair, G. W. (1994) Isotope and trace element characteristics of a super-fast spreading ridge. East Pacific rise, 13–23°S. *Earth Planet. Sci. Lett.* **121**, 173–193.
Makishima, A. and Nakamura, E. (1997) Suppression of matrix effects in ICP-MS by high power operation of ICP: application to precise determination of Rb, Sr, Y, Cs, Ba, REE, Pb, Th and U at ng g^{-1} levels in milligram silicate samples. *Geostand. Geoanal. Res.* **21**, 306–309.
Makishima, A., Nakamura, E. and Nakano, T. (1999) Determination of zirconium, niobium, hafnium and tantalum at ng g^{-1} levels in geological materials by direct nebulisation of sample HF solution into FI-ICP-MS. *Geostand. Geoanal. Res.* **28**, 7–20.
McDade, P., Blundy, J. D. and Wood, B. J. (2003) Trace element partitioning on the Tinaquillo Lherzolite solidus at 1.5 Gpa. *Phys. Earth Planet. Inter.* **139**, 129–147.
Miyaji, N. (1988) History of younger Fuji volcano. *J. Geol. Soc. Japan* **94**, 433–452.
Moriguti, T. and Nakamura, E. (1998) Across-arc variation of Li isotopes in lavas and implications for crust/mantle recycling at subduction zones. *Earth Planet. Sci. Lett.* **163**, 167–174.
Nakajima, J. and Hasegawa, A. (2006) Anomalous low-velocity zone and linear alignment of seismicity along it in the subducted Pacific slab beneath Kanto, Japan: Reactivation of subducted fracture zone? *Geophys. Res. Lett.* **33**, L16309, doi:10.1029/2006GL026773.
Nakamura, K. (1964) Volcano-stratigraphic study of Oshima

volcano, Izu. *Bull. Earthq. Res. Inst.* **42**, 649–728.

Niihori, K., Tsukui, M. and Kawanabe, Y. (2003) Evolution of magma plumbing system of Miyakejima volcano. *Bull. Volcanol. Soc. Japan* **48**, 387–405 (in Japanese with English abstract).

Nishio, Y., Nakai, S., Yamamoto, J., Sumino, H., Matsumoto, T., Prikhod'ko, V. S. and Arai, S. (2004) Lithium isotopic systematics of the mantle-derived ultramafic xenoliths: implications for EM1 origin. *Earth Planet. Sci. Lett.* **217**, 245–261.

Pearce, J. A. and Parkinson, I. J. (1993) Trace element models for mantle melting: application to volcanic arc petrogenesis. *Magmatic Processes and Plate Tectonics* (Prichard, H. M. *et al*., eds.), Geol. Soc. Spec. Publ. 76, 373–403, Geological Society.

Pin, C. and Zalduegui, J. F. S. (1997) Sequential separation of light rare-earth elements, thorium and uranium by miniaturized extraction chromatography: Application to isotopic analyses of silicate rocks. *Anal. Chim. Acta* **339**, 79–89.

Plank, T., Kelley, K. A., Murray, R. W. and Stern, L. Q. (2007) Chemical composition of sediments subducting at the Izu-Bonin trench. *Geochem. Geophys. Geosyst.* **8**, Q04I16, doi:10.1029/2006GC01444.

Sigmarsson, O., Condomines, M., Morris, J. D. and Harmon, R. S. (1990) Uranium and ^{10}Be enrichments by fluids in Andean arc magmas. *Nature* **346**, 163–165.

Sigmarsson, O., Gill, J. and Holden, P. (2006) U–Th–Ra and U–Pa disequilibria in Izu-arc: the interplay of depleted mantle wedge and sediment. *Eos* (Transactions, American Geophysical Union), **83**, Fall Meeting Supplement, Abstract T71F-06.

Straub, S. M. and Layne, G. D. (2002) The systematics of boron isotopes in Izu arc front volcanic rocks. *Earth Planet. Sci. Lett.* **198**, 25–39.

Sun, S.-S. and McDonough, W. F. (1989) Chemical and isotopic systematics of oceanic basalts: implications for mantle composition and processes. *Geol. Soc. Spec. Publ.* **42**, 313–345.

Suyehiro, K., Takahashi, N., Ariie, Y., Yokoi, Y., Hino, R., Shinohara, M., Kanazawa, T., Hirata, N., Tokuyama, H. and Taira, A. (1996) Continental crust, crustal underplating, and low-Q upper mantle beneath an ocean island arc. *Science* **272**, 390–392.

Taira, A., Saito, S., Aoike, K., Morita, S., Tokuyama, H., Suyehiro, K., Takahashi, N., Shinohara, M., Kiyokawa, S., Naka, J. and Klaus, A. (1998) Nature and growth rate of the Northern Izu-Bonin (Ogasawara) arc crust and their implications for continental formation. *The Island Arc* **7**, 395–407.

Takahashi, M., Hasegawa, Y., Tsukui, M. and Nemoto, Y. (1991) Evolution of magma-plumbing system beneath Fuji volcano: on the view point of whole-rock chemistry. *Bull. Volcanol. Soc. Japan* **36**, 281–296 (in Japanese with English abstract).

Takahashi, N., Suyehiro, K. and Shinohara, M. (1998) Implications from the seismic crustal structure of the northern Izu-Bonin arc. *The Island Arc* **7**, 393–394.

Tatsumi, Y. and Hanyu, T. (2003) Geochemical modeling of dehydration and partial melting of subducting lithosphere: Toward a comprehensive understanding of high-Mg andesite formation in the Setouchi volcanic belt, SW Japan. *Geochem. Geophys. Geosyst.* **4**, 1081, doi:10.1029/2003GC000530.

Tatsumi, Y., Murasaki, M. and Nohda, S. (1992) Across-arc variation of lava chemistry in the Izu-Bonin arc: identification of subduction components. *J. Volcanol. Geotherm. Res.* **49**, 179–190.

Taylor, R. N. and Nesbitt, R. W. (1998) Isotopic characteristics of subduction fluids in an intra-oceanic setting, Izu-Bonin Arc, Japan. *Earth Planet. Sci. Lett.* **164**, 79–98.

Tepley, F. J., III, Lundstrom, C. C., Gill, J. B. and Williams, R. W. (2006) U–Th–Ra disequilibria and the time scale of fluid transfer and andesite differentiation at Arenal volcano, Costa Rica (1968–2003). *J. Volcanol. Geotherm. Res.* **157**, 147–165.

Tollstrup, D. L. and Gill, J. B. (2005) Hafnium systematics of the Mariana arc: Evidence for sediment melt and residual phases. *Geology* **33**, 737–740.

Tsukui, M., Niihori, K., Kawanabe, Y. and Suzuki, Y. (2001) Stratigraphy and formation of Miyakejima volcano. *J. Geogr.* **110**, 156–167 (in Japanese with English abstract).

Turner, S., Hawkesworth, C., Rogers, N., Bartlett, J., Worthington T., Hergt, J., Pearce, J. and Smith, I. (1997) ^{238}U–^{230}Th disequilibria, magma petrogenesis, and flux rates beneath the depleted Tonga–Kermadec island arc. *Geochim. Cosmochim. Acta* **61**, 4855–4884.

Turner, S., Bourdon, B. and Gill, J. (2003) Insights into magma genesis at convergent margins from U-series isotopes. *Rev. Mineral. Geochem.* **52**, 255–315.

van Wastrenen, W., Blundy, J. and Wood, B. (1999) Crystal-chemical controls on trace element partitioning between garnet and anhydrous silicate melt. *Am. Mineral.* **84**, 838–847.

Watanabe, S., Widom, E., Ui, T., Miyaji, N. and Roberts, A. M. (2006) The evolution of a chemically zoned magma chamber: The 1707 eruption of the Fuji volcano, Japan. *J. Volcanol. Geotherm. Res.* **152**, 1–19.

White, W. M., Hofmann, A. W. and Puchelt, H. (1987) Isotope geochemistry of Pacific mid-ocean ridge basalt. *J. Geophys. Res.* **92**, 4881–4893.

Yamamoto, T., Soya, T., Suto, S., Uto, K., Takada, A., Sakaguchi, K. and Ono, K. (1991) The 1989 submarine eruption off eastern Izu Peninsula, Japan: ejecta and eruption mechanisms. *Bull. Volcan.* **53**, 301–308.

Yokoyama, T., Kobayashi, K., Kuritani, T. and Nakamura, E. (2003) Mantle metasomatism and rapid ascent of slab components beneath island arcs: Evidence from ^{238}U–^{230}Th–^{226}Ra disequilibria of Miyakejima volcano, Izu arc, Japan. *J. Geophys. Res.* **108**, doi:10.1029/2002 JB002103.

Yokoyama, T., Kuritani, T., Kobayashi, K. and Nakamura, E. (2006) Geochemical evolution of a shallow magma plumbing system during the last 500 years, Miyakejima volcano, Japan: Constraints from ^{238}U–^{230}Th–^{226}Ra systematics. *Geochim. Cosmochim. Acta* **70**, 2885–2901.

Yoshida, T., Yamasaki, S. and Tsumura, A. (1992) Determination of trace and ultra-trace elements in 32 international geostandards by ICP-MS. *J. Min. Pet. Econ. Geol.* **87**, 107–122.

Yoshimoto, M., Fujii, T., Kaneko, T., Yasuda, A. and Nakada, S. (2004) Multiple magma reservoirs for the 1707 eruption of Fuji volcano, Japan. *Proc. Japan Acad.* **B.80**, 103–106.

Appendix 1. Results of trace element analyses of geological standard sample of JB2 and comparisons with GSJ recommended values and results from other groups

	Average	RSD(%)	*n*	GSJ recommended values[1]	Yoshida *et al.* (1992)	Makishima and Nakamura (1997)
Rb	6.61	6.3	3	7.37	6.59	7.13
Sr	178	8.8	3	178	176.8	177
Zr	45.6	9.7	3	51.2	44.8	46 2
Nb	0.475	5.9	2	1.58	0.80	0.45[2]
Cs	0.814	4.3	3	0.85	0.78	0.794
Ba	222	5.5	3	222	211.9	229
La	2.43	7.0	3	2.35	2.41	2.19
Ce	6.68	6.3	3	6.76	6.60	6.43
Pr	1.21	7.0	3	1.01	1.11	1.13
Nd	6.19	4.0	3	6.63	6.74	6.39
Sm	2.24	3.9	3	2.31	2.38	2.27
Eu	0.808	1.6	3	0.86	0.85	0.86
Gd	3.03	2.5	3	3.28	3.01	3.12
Tb	0.544	3.0	3	0.60	0.60	0.592
Dy	3.69	5.2	3	3.73	3.85	4.13
Ho	0.811	5.5	3	0.75	0.86	0.898
Er	2.44	4.9	3	2.60	2.50	2.47
Tm	0.356	5.5	3	0.41	0.42	0.397
Yb	2.42	4.8	3	2.62	2.63	2.60
Lu	0.360	6.7	3	0.40	0.39	0.397
Hf	1.42	5.1	3	1.49	1.40	1.46[2]
Pb	5.37	2.4	3	5.36	4.95	5.28
Th[3]	0.270	3.6	3	0.35	0.25	0.277
U[3]	0.173	4.0	3	0.18	0.10	0.166

Concentrations are reported in ppm.
[1]Imai et al. (1995).
[2]Makishima et al. (1999).
[3]U and Th abundances were determined by an ICP-MS with a quarupole mass analyzer.

Appendix 2. Compositions of the components used for model calculations

	PAC[1]	PSP[2]	Sediment[3]	Sediment melt I[4]	Sediment melt II[5]	Modified PAC[6]	Modified PSP[7]	AOC[8]	Fluid I[9]	Fluid II[10]
Sr	14.8	23.8	136	260	260	16	25	122	213	229
Nd	1.24	1.74	25.2	59.0	62.8	1.53	2.02	10.4		1.59
Th	0.018	0.052	4.39	14.2	21	0.089	0.119	0.21	0.156	0.131
U	0.07	0.02	0.92	4.90	5.17	0.031	0.044	0.19	0.814	0.209
($^{238}U/^{232}Th$)	1.18	1.17	0.638	1.05	0.75	1.08	1.13	2.75	15.9	4.86
($^{230}Th/^{232}Th$)[11]	1.18	1.17	0.638	1.05	0.75	1.08	1.13	2.75	2.12	2.12
$^{87}Sr/^{86}Sr$	0.7025	0.7029	0.70956	0.70956	0.70956	0.70307	0.70325	0.704769	0.704873	0.704873
$^{143}Nd/^{144}Nd$	0.51315	0.51307	0.51231	0.51231	0.51231	0.51299	0.51296	0.513153	0.513109	0.513109

[1]Initial compositions of the mantle were estimated following Ishizuka et al. (2003). Trace element concentrations were calculated assuming 15% batch melting of spinel lherzolite produced the lavas with the composition of N-MORB in Sun and McDonough (1989). Isotopic composition is based on the data from White et al. (1987) and Mahoney et al. (1994) at $^{143}Nd/^{144}Nd = 0.513150$. Mineral/melt partition coefficients are from compilation of Pearce and Parkinson (1993) and Bedard (1999).

[2]Initial compositions of the mantle were estimated following Ishizuka et al. (2003). Trace element concentrations were calculated assuming 15% batch melting of spinel lherzolite produced the average compositions of the lavas from Shikoku Basin (Hickey-Vargas, 1998). Isotopic compositions are estimated from the compositions of the Shikoku Basin lavas (Hickey-Vargas, 1991).

[3]Bulk compositions of Izu trench sediment based on ODP1149 (Plank et al., 2007).

[4]Melt compositions are for batch, non-modal melting with modal proportions of 0.6/0.39/0.01/0.00003/0.00000034 and melting proportions of 0.6/0.4/0/0/0 for clinopyroxene, garnet, rutile, zircon and monazite, respectively. Mineral/melt partition coefficients for Sr, Nd, Th and U are 0.074, 273, 0.021, 0.018 for clinopyroxene (McDade et al., 2003); 0.002, 0.008, 0.0046, 0.011 for garnet (van Westrenen et al., 1999); 0, 0, 0.0000004, 0 for rutile (Blundy and Wood, 2003; Tatsumi and Hanyu, 2003), 0, 0.2, 17, 100 for zircon (Blundy and Wood, 2003); and 0, 76400, 293000, 2900 for monazite (Bea et al., 1994).

[5]Melt compositions are for batch, non-modal melting with modal proportions of 0.6/0.4 and melting proportions of 0.6/0.4 for clinopyroxene, garnet, respectively.

[6]PAC mantle modified by the addition of 0.5% sediment melt I.

[7]PSP mantle modified by the addition of 0.5% sediment melt I.

[8]Bulk compositions of altered oceanic crust (AOC) on ODP1149 (Hauff et al., 2003; Kelley et al., 2003; Plank et al., 2007).

[9]Chemical compositions of mixed fluid were calculated by assuming 2% fluid equilibrated with mixture of altered oceanic crust and sediment with a proportion of 0.98:0.02 and with rock/fluid partition coefficients of eclogite at 3 GPa from table 2 in Turner et al. (2003) and Brenan et al. (1995). Sr and Nd isotopic compositions were those of the mixture.

[10]Chemical compositions of mixed fluid were calculated by assuming 2% fluid equilibrated with mixture of altered oceanic crust and sediment with a proportion of 0.98:0.02 and with rock/fluid partition coefficients of eclogite at 4 Gpa, 800°C in Kessel et al. (2005). Sr and Nd isotopic compositions were those of the mixture.

[11]($^{230}Th/^{232}Th$) of each component except the two fluid components were calculated assuming that each component is in radioactive equilibrium. ($^{230}Th/^{232}Th$) of the two fluid components are those of their source materials.